



HAL
open science

An experimental study of bathymetry influence on turbulence at a tidal stream site

Maria Ikhennicheu, Philippe Druault, Benoît Gaurier, Gregory Germain

► To cite this version:

Maria Ikhennicheu, Philippe Druault, Benoît Gaurier, Gregory Germain. An experimental study of bathymetry influence on turbulence at a tidal stream site. EWTEC 2017 - 12th European Wave and Tidal Energy Conference, Sep 2017, Cork, Ireland. hal-02140512

HAL Id: hal-02140512

<https://hal.sorbonne-universite.fr/hal-02140512>

Submitted on 27 May 2019

HAL is a multi-disciplinary open access archive for the deposit and dissemination of scientific research documents, whether they are published or not. The documents may come from teaching and research institutions in France or abroad, or from public or private research centers.

L'archive ouverte pluridisciplinaire **HAL**, est destinée au dépôt et à la diffusion de documents scientifiques de niveau recherche, publiés ou non, émanant des établissements d'enseignement et de recherche français ou étrangers, des laboratoires publics ou privés.

An experimental study of bathymetry influence on turbulence at a tidal stream site

Maria Ikhennicheu*, Philippe Druault[†], Benoît Gaurier*, Grégory Germain*

*Marine Structure Laboratory, IFREMER, 150 Quai Gambetta, 62200 Boulogne sur Mer. France

E-mail: gregory.germain@ifremer.fr

[†]Institut Jean le Rond d'Alembert, UPMC, Paris. France

E-mail: philippe.druault@upmc.fr

Abstract—This study aims at completing the lack of knowledge on turbulence characteristics in high flow velocity areas like those suitable for marine energy application. We present in this paper the methodology used to recreate the turbulent phenomenon existing in the Raz Blanchard by representing significant seabed elements in a circulating tank.

The first set of experiment was achieved for the flow measurement results obtained around a wall-mounted cube at $Re = 2.5 \times 10^5$ and $Fr = 0.23$, in representative *in-situ* conditions. These measurements have been done for different kinds of flow from laminar to highly turbulent (turbulence intensity rate from 3 to 15%) in both horizontal and vertical planes, using LDV and PIV measurements. The study shows similar results for the low turbulence intensity cases in terms of flow topology (stagnation point, recirculation length and energetic considerations). It is also shown that the wall-mounted cube does not create the structures observed *in-situ*. Indeed, the structures of interest here are very persistent macroturbulences that may be generated at the sea floor and erupt at the free surface. The possibility that these structures could be Kolk vortices is considered. In order to recreate such phenomena, the idea of placing an inclined floor downstream of the cube is investigated. The results show that turbulent structures are significantly impulsed by a 6.5° inclined floor and rise up to 13% higher in the water column. The question of the aspect ratio of the obstacle is also investigated. Furthermore, numerical simulations on dune with similar incoming flow conditions show encouraging results and indicate the path for further experimental testing.

Index Terms—Marine energy, turbulence, experimental trial, flow measurement

I. INTRODUCTION

The idea of harvesting energy from the sea dates back to antiquity, however it is only recently that industrial projects have started to emerge (see [1]). There is a strong tidal potential in France (as described in [2]): over 20% of the European potential is located in French water. A project of a pilot farm was started in the Raz Blanchard (Alderney Race) that presents currents up to 5 m/s. Surveys performed in the Raz-Blanchard give access to the bathymetry [3] showing a very uneven aspect with a 5 m mean variation (e.g. *in situ*: $Re = 2.5 \times 10^7$). On the sea surface, large scale boils can be observed and their origin remains unknown. They are visible far from the coast and for all wave conditions, hence these structures cannot be created by the coast only, some must originate in the sea floor (represented in figure 1) and go up the water column. They indicate a high turbulence rate and

seem to be the most relevant turbulent phenomenon at the sea bottom, where turbines are meant to be installed. Turbulence can have a major impact on the tidal turbines (on their production and on the structural fatigue [4]), hence the origin and characterization of the turbulence in such area is essential.

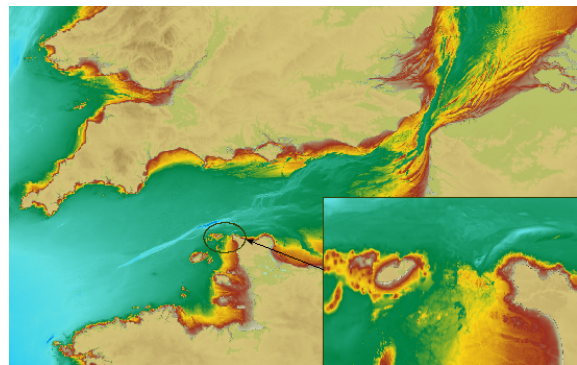


Fig. 1: Bathymetry of the English Channel with a zoom of the Raz Blanchard area, SHOM [3]

The apparition of boils at the water surface is frequent, mostly in estuaries or rivers ([5] & [6]). An extensive list of the related research was made in [7]. They concluded that, however this phenomenon was mostly studied for river cases, it exists at sea. These structures were first described in [8] on dunes and were named Kolk vortices, this denomination will be used for the rest of the paper. They are horseshoe shaped vortices that are created at the reattachment of the recirculation zone downstream of the obstacle. Because of the temporal turbulent pattern of the upstream flow, the reattachment line has an intermittent behaviour [6]. The lateral instability of the reattachment line creates highly energetic structures that go up to the surface. The Kolk vortices then erupt at the surface creating boils. This could be the explanation of the large scale eddies visible at the sea surface in the Raz Blanchard.

Kolk vortices were successfully reproduced in a tank in [9], they were working at $Re = 1.7 \times 10^4$, $Fr = 0.29$ and with a ratio $\frac{Dune\ height}{depth} = \frac{1}{20}$ which are similar conditions to ours (except for the lower Reynolds number). Experiments were also conducted in [10], where the impact of bathymetric

variations (various patterns of dunes or cubes) was studied by observing the free surface (still for lower Reynolds number $Re < 10^3$). In [11], they considered in addition the sediment transport, that however part of the process, will not be considered here. Finally, we can highlight the numerical studies [12] or [13] on oceanic dunes.

The representation of real life structures in experimental set-ups has been extensively studied for various geometries like dunes, cavities, cylinders, Ahmed bodies or hemispheres. Before trying to reproduce complex structure, we chose to introduce the topic by studying a known and simple structure: a cube. The wall-mounted cube is a common obstacle studied in a wind tunnel or a water tank. However, fewer were achieved at high Reynolds number ($Re > 10^5$). We count the studies performed in [14] at $Re = 1.8 \times 10^6$ or [15] going up to $Re = 10^5$, both in wind tunnels. The IFREMER tank presents the advantage of achieving high Reynolds number in water. Furthermore, sea states detailed in [4] show turbulence intensities varying between 3% up to 15%, a range that can also be achieved in this tank [4].

Among the first to ever characterize the flow around a wall-mounted cube and describe its wake, we can quote the following studies: [16] and [17]. In keeping with their work, [15] highlighted the importance of the boundary layer thickness δ . It is fundamental to know where the obstacle intersects the boundary layer to characterize the incoming stress field. The interesting effect of flow incidence on the wake of the cube was studied in [18].

The present study is placed in a larger project that includes numerical work and *in-situ* measurements. The database established in this study has to be consistent with *in-situ* measurements and the real bathymetry. This work is also meant to create a database for numerical work ([19] & [20]). So far, no data in conditions close enough to the Raz Blanchard exist (i.e. consistent bathymetry, similar Froude number and high Reynolds number ($Re > 10^5$)). Finally, the obstacles tested in the tank should be realizable in the numerical simulations conducted in parallel to these tests.

After presenting the experimental set-up and the incoming flow conditions, the results on the wall-mounted cube will be presented with maps of mean and fluctuating velocities, energy consideration and through a frequency analysis. A comparison between two low turbulence rate cases will be made and more details on the degraded flow case will be presented. Then, the presence of an inclined floor downstream of the cube will be presented along with some of the first numerical and experimental results.

II. EXPERIMENTAL SET-UP

The tests are carried out in the circulating flume tank of IFREMER in Boulogne-sur-mer presented in figure 2. The flow velocity is studied on its three instantaneous components (U, V, W) along the (X, Y, Z) directions (Fig. 3). The incoming flow is assumed to be steady and uniform. Various turbulence intensities are achievable in the tank. Turbulence

intensity TI in the incoming flow is defined in eq.1, where an overbar indicates the time average. In this paper, the Reynolds decomposition will be used, the instantaneous velocity equals its mean value and a fluctuation term: $U = \bar{U} + u'$ (in the rest of the paper, $\bar{U} = U_{mean}$).

$$TI_{\infty}(3D) = 100 \sqrt{\frac{\frac{1}{3}(\overline{u'^2} + \overline{v'^2} + \overline{w'^2})}{\overline{U_{\infty}^2} + \overline{V_{\infty}^2} + \overline{W_{\infty}^2}}} \quad (1)$$

According to the experiments carried out in the same tank [4], the natural ambient TI in the tank is 15% (this case will be dealt with later in the paper as a degraded flow case). By means of grid and honeycomb (that acts as a flow straightener) placed at the inlet of the working section (see fig. 2), lower TI can be achieved: $TI = 3\%$ using the grid and the honeycomb and $TI = 5\%$ using only the honeycomb. $TI = 3\%$ will be referred to as case 1a, $TI = 5\%$ as case 1b and $TI = 15\%$ as case 2.

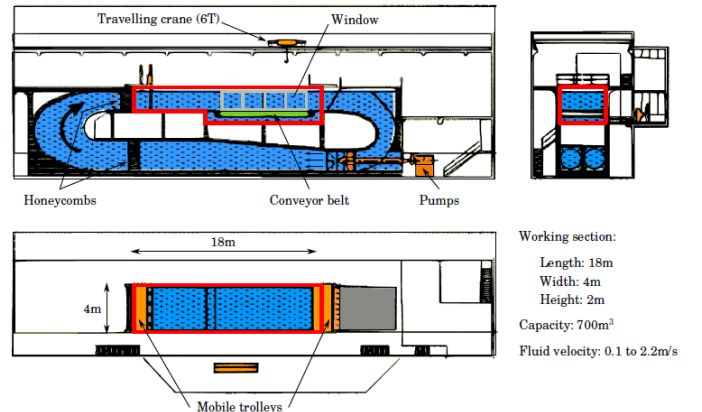


Fig. 2: IFREMER Flume tank (Boulogne-sur-Mer)

The flow around a the wall-mounted cube is studied (fig. 3) with dimensions chosen to be representative of the Raz Blanchard. Its height: $H = 250 \text{ mm}$ represents the mean bathymetric variation in the area of interest at a 1:20 scale. The scale must be so that the Reynolds number is high and the blockage ratio is low $\tau = \frac{\text{cross section of the cube}}{\text{cross section of the tank}} < 10\%$ (in order to limit the tank border effects). The current velocity is chosen in Froude similitude considerations, in order to respect the interaction between the sea bottom and the free surface.

	U_{∞} [m/s]	Rugosity height [m]	Depth [m]	Re	F_r
Raz Blanchard	5	5	40	2.5×10^7	0,25
Flume tank	1	0,25	2	2.5×10^5	0,23

TABLE I: *in situ* and experimental conditions

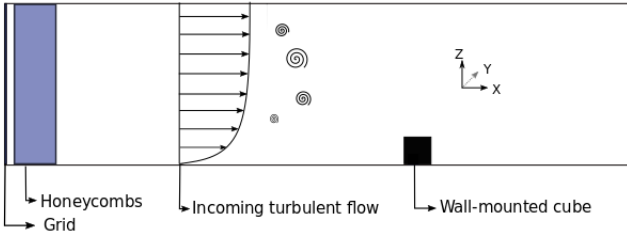


Fig. 3: Representation of the cube in the tank

Two measurement techniques are used in this study, they are illustrated on the cube in figure 4. For both techniques, the tank is seeded with $10 \mu m$ diameter micro-particles. The LDV (Laser Doppler Velocimetry) acquisitions are made using a 2D DANTEC FiberFLOW system. The probe is positioned both horizontally ((U, V) measurements) and vertically ((U, W) measurements) at various streamwise positions : $x/H = [-2, -1, 0, 1, 2, 3]$ and along the Z or Y axis depending on the case. With LDV measurements, the acquisition frequencies are not constant (between $15 Hz$ and $30 Hz$ for the spanwise velocity component), a re-sampling is done in the post processing. Based on previous works performed in the tank ([21]), we re-sample using the mean sample rate of the set of measurements considered. For the PIV (Particle Image Velocimetry), a Nd-YAG laser GEMINI-LIKE is used with a Camera FLOWSENS EO-2M $1600 pix \times 1200 pix$ that makes double images separated by $800 \mu s$. PIV acquisitions are made for $150s$ or more. The data are post processed with the software DYNAMIC STUDIO. To get rid of noise, the mean image is first subtracted to all images. Then, the displacement of particles is calculated using a Cross-Correlation and outliers are replaced with the Universal Outlier Detection. This method uses interrogation windows of $32 pix \times 32 pix$. Two configurations are used for the PIV measurements: for horizontal planes (laser lightening the $(z/H = 0.7)$ plane of the fluid and camera placed above the cube, perpendicularly to the laser plane) and for vertical planes (laser lightening the $(y = 0)$ plane of the fluid and camera positioned beside the cube). The dimensions of the planes for both cases are given in table II. For one set of measurement, 6 to 9 measurement planes are carried out. The experimental conditions of each set of PIV measurements are summarised in table II.

To avoid any statistical convergence issue in LDV measurements, the acquisition time is set to 6 minutes outside



Fig. 4: Picture of the cube in the tank with LDV and PIV shooting

Orientation	TI(%)	Plane position	N° of plane	Planes size [mm]	Precision [mm]
Vertical	3, 5 & 15	$y/H = 0$	9	350×275	$\Delta x = \Delta z = 0.43$
Horizontal	3 & 15	$z/H = 0.7$	6	737×553	$\Delta x = \Delta z = 0.23$

TABLE II: Sets of PIV measurements

of the wake and 4 minutes elsewhere.

As highlighted in the literature ([15] and [14]), the boundary layer thickness $\delta = \delta_{95}$ (calculated as $U(z = \delta_{95}) = 0.95 \times U_{\infty}$) is of interest here in order to characterize the incoming profile on the obstacle. δ is calculated upstream of the cube at $x/H = -2$. For case 1a, we find $\delta/H = 1.3$ and for case 1b, $\delta/H = 1.6$. Free stream turbulence has the primary effect of increasing δ (see [14]).

III. WAKE OF A WALL-MOUNTED SINGLE CUBE

The wake of the cube is studied for various incoming conditions, $TI = 3\%$ (case 1a), $TI = 5\%$ (case 1b) and a degraded turbulent flow (case 2) with a spatial and temporal description.

A. Spatial characterization of the wake

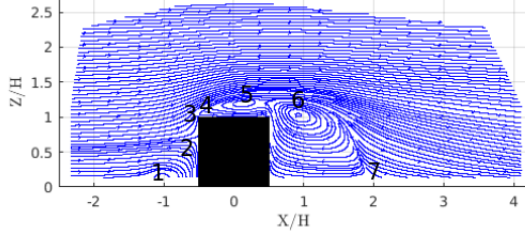
1) *For a low turbulence incoming flow:* The flow around an obstacle shows common characteristics for all geometric forms. We present the streamlines in vertical PIV measurements in figure 5(a). The various events happening to a flow around a wall-mounted cube are listed in table III, inspired by the work done for an hemisphere [22]. This description is also applicable for the horizontal view in figure 5(b).

- | |
|--|
| <ol style="list-style-type: none"> 1) Development of a horseshoe vortex and apparition of the upstream recirculation area (x_{us}). 2) Stagnation point on the upstream face of the cube (z_{st}). 3) Fluid acceleration. 4) Fluid separation at the leading edges of the cube. 5) Separation of the flow between the outer steady region and the recirculation area downstream of the cube. 6) Shear layer (that can lead to Kelvin-Helmholtz instabilities). 7) Reattachment point (x_{ds}). |
|--|

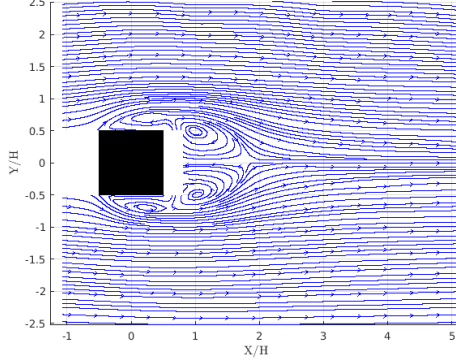
TABLE III: Description of the flow around an obstacle

The results for case 1a, in terms of mean velocities, are presented in figure 6 and 7¹. Both the vertical and horizontal U_{mean} planes illustrate the description of the wake in table III. We can see the recirculation areas (where $U_{mean} < 0$) and the transition between the recirculation area (in blue) and the steady outer flow (in red). The spanwise velocities: W_{mean} and V_{mean} illustrate the same process. In the incoming flow, the average spanwise velocity is zero and it increases or decreases around the recirculation area. This can be observed

¹The white parts are area where the laser light was not powerful enough for the camera to detect particles



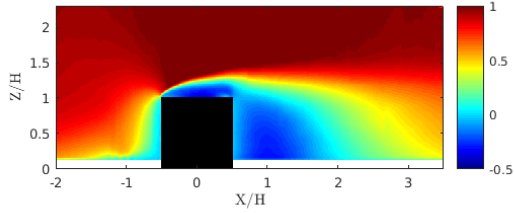
(a) Streamlines at (case 1a), vertical field



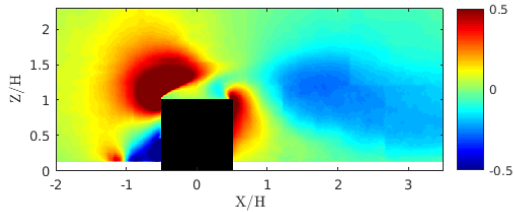
(b) Streamlines (case 1a), horizontal field

Fig. 5: Streamlines at $TI = 3\%$ (case 1a), different views

in figure 7(b): along $x = 2H$, $V_{mean} = 0$ at $y/H = 1.5$ in the outer region. The fluid is then directed towards the recirculation area (see fig. 5(b)), then causes a deficit in the spanwise velocity: $V_{mean} < 0$. When the fluid reaches $y/H = 0$, between the two contra-rotating vortices (see fig. 5(b)), $V_{mean} = 0$. The same phenomenon happens backwards when y/H decreases below 0.

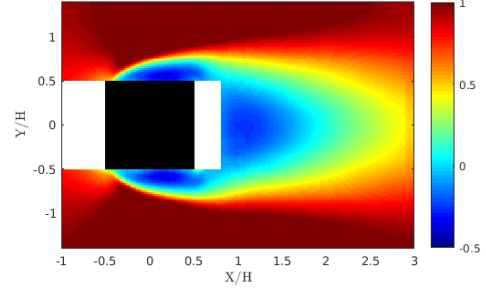


(a) U_{mean} , (case 1a)

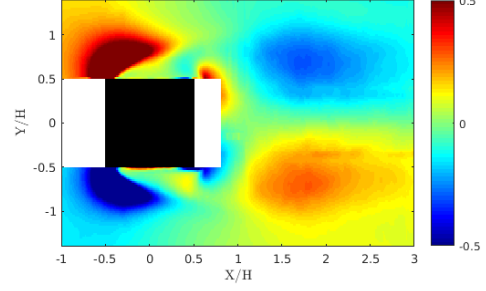


(b) W_{mean} , (case 1a)

Fig. 6: Mean speed, case 1a ($TI = 3\%$), vertical field



(a) U_{mean} , (case 1a)



(b) V_{mean} , (case 1a)

Fig. 7: Mean speed, case 1a ($TI = 3\%$), horizontal field

The stress tensor's components are calculated as $\tau_{uu} = \frac{\overline{u'u'}}{U_\infty^2}$, $\tau_{vv} = \frac{\overline{v'v'}}{U_\infty^2}$ and $\tau_{ww} = \frac{\overline{w'w'}}{U_\infty^2}$ for the diagonal terms and the shear terms are: $\tau_{uv} = \frac{\overline{u'v'}}{U_\infty^2}$, $\tau_{vw} = \frac{\overline{v'w'}}{U_\infty^2}$ and $\tau_{uw} = \frac{\overline{u'w'}}{U_\infty^2}$. Maps of the Reynolds shear stress (τ_{uw} and τ_{uv}) are provided in figures 8 and 9. This quantity illustrates the shift between the steady flow and the recirculation zones where the energy is dissipated by turbulent agitation. In figure 8, $\tau_{uw} > 0$ (in red in the map) at the leading edge of the cube, it indicates the wake separation. Downstream, τ_{uw} decreases (in blue in the map) when the shear increases. The same phenomenon can be observed in figure 9: $\tau_{uv} > 0$ at the top leading edge of the cube and then increases. The opposition of the signs is an indication of the counter-rotating vortices existing in the wake of the cube (see fig. 5(b)). The absolute value of the Reynolds shear stress increases up to the reattachment point ($x/H = 1.9$) and then decreases. The Reynolds shear stress maps allow to see the extend of the wake of the cube. It is clear in figures 8 and 9 that the measurements do not go far enough to conclude on the streamwise extend of the wake. In [14], they showed that the wake of a cube in a turbulent flow can go up to $x/H = 10$ which is far from what we are presenting here.

2) *Comparison with a higher turbulence level case:* Experiments with the same experimental set-up are conducted for the case 1b. The flow behaviour in cases 1a and 1b is very similar as illustrated in figure 10. As mentioned before, there are three recirculation areas on the wake of a cube: one upstream (x_{us}), one on the top (x_{top}) and one downstream (x_{ds}). For the cases 1a and 1b, we find the same

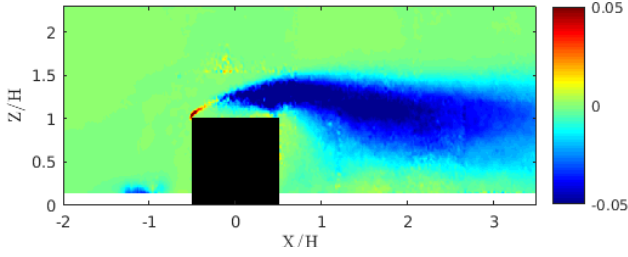


Fig. 8: τ_{uw} (case 1a), vertical field

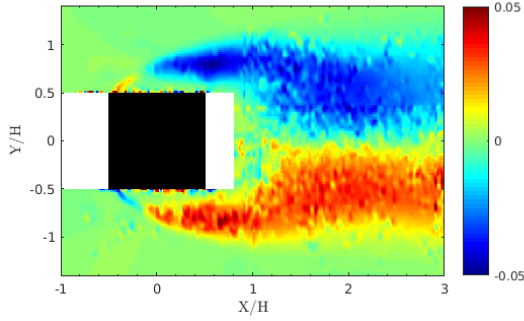


Fig. 9: τ_{uw} (case 1a), horizontal field

reattachment point locations: $x_{us}/H = -0.7$, $x_{top}/H = 0.4$ and $x_{ds}/H = 1.9$ (this last result is similar to the 1.9 found in [14] for $Re = 1.8 \times 10^6$ in air). The stagnation point on the frontal face of the cube z_{st} is also located at the same location for both cases: $z_{st}/H = 0.7$. These results are consistent with the conclusions in [14] of $z_{st}/H = 0.65$. The independence of x_{ds} with changing incoming turbulence intensity are validated by both [14] and our results. Furthermore, for experiments at $Re \sim 10^4$ ([16]), the results stay similar: x_{ds} seems to also be independent of the incoming Reynolds number (as long as $Re > 10^4$). In addition, it was found in [15] that, for high Re ($Re > 4000$), the turbulent flow achieves a certain Reynolds number independence, thus the results found in a tank for $Re = 2.5 \times 10^5$ should be applicable in the Raz Blanchard case ($Re = 2.5 \times 10^7$) as well. Nevertheless, the same studies have highlighted that incoming turbulence has an impact on the length of the wake of the cube, quantity that is not studied here.

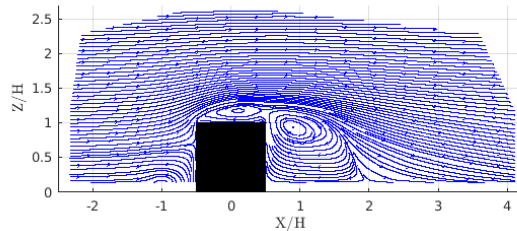


Fig. 10: Streamlines at $TI = 5\%$ (case 1b), vertical PIV field

Using the mean streamwise velocity PIV measurements, we calculate the area of influence of the cube in the spanwise direction of the flow: y_i and z_i . The calculation are conducted

in a similar way to the boundary layer calculations (i.e. $U_{z=z_i} = 0.95 \cdot U_\infty$) and at $x/H = 2$. The results are similar for both 1a and 1b cases: $z_{i,1}/H = 1.5$, and in the Y direction (case 1a): $y_{i,1}/H = 1.2$. These values are in the range of what can be found in the literature.

Some differences between the low turbulence cases are noticed whilst looking at the PIV maps of mean velocities. A more extensive analysis allows us to refine the comparison. As expected, the values of τ_{uu} , τ_{vv} and τ_{ww} are higher in the undisturbed incoming flow in case 1b. The main area of interest is the wake of the cube and the TI impact on the flow behaviour past the obstacle. The mean velocities maps show that the wake in case 1b is thinner and shorter. To have a better understanding of the differences between both cases, we look at the average Reynolds shear stress profiles: τ_{uw} at $x/H = 1$ and $x/H = 3$ presented in figure 11. Underneath the strong shear layer (as can be seen in figure 8 for $z/H < 0.5$), τ_{uw} is stronger for case 1b. However, even though the peak occurs at the same altitude for both positions, it is weaker for case 1b. Furthermore, at $(x/H = 3, z/H = 1.5)$, $\tau_{uw}(1a) \sim 2 \times \tau_{uw}(1b)$. This illustrates the thinning of the shear layer at higher turbulence intensity: the wake of the cube dissipates faster when the incoming turbulence increases.

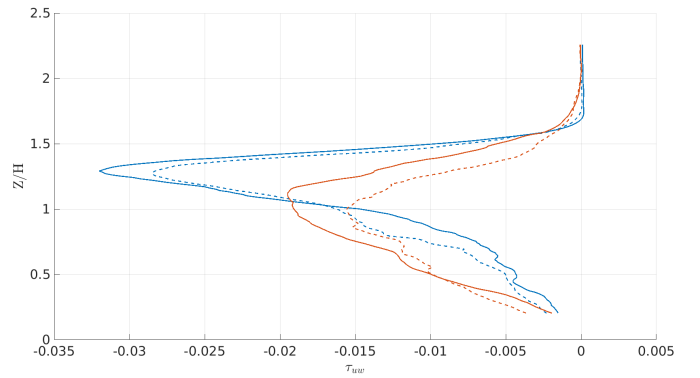


Fig. 11: τ_{uw} for case 1a (solid line) and case 1b (dashed line) at $x/H = 1$ (blue) and $x/H = 3$ (orange)

3) *Case of a degraded incoming flow:* As mentioned earlier, the natural state of the flow in the tank (i.e. without honeycomb nor grid) has a $TI = 15\%$. The flow also presents all scales of eddies including some large scale recirculations (around the size of the working section in the tank). It causes the apparition of a 15° incidence angle on the incoming flow on the studied area (around the cube)² visible in figure 12. It is assumed that, even if it might not be the case on the whole tank, the state of the flow is preserved on the limited studied area around the cube. Hence, the specific case of $TI = 15\%$ (case 2) will be considered as a degraded flow, closer to a real in-situ case.

Figure 13 presents the map of U_{mean} . The wake behind the cube has a different aspect than for cases 1a and 1b

²This angle does not exist for cases 1a and 1b since the honeycomb straightens the flow.

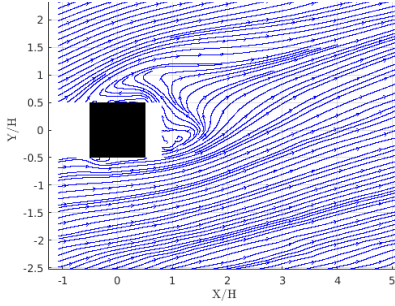


Fig. 12: Streamlines ($TI = 15\%$), horizontal field

(the wake was drop shaped, see fig. 7(a)). The flow around a wall-mounted cube at incidence was studied in [18] and [23]. Their studies, although at lower Reynolds number ($Re \approx 10^4$) and lower turbulence rate (under 1%), showed that the downstream aspect of the wake of the cube changes considerably depending on the incidence. Both showed that the drop shape of the cube's wake at $\alpha = 0^\circ$ disappears at $\alpha = 15^\circ$. At $\alpha = 0^\circ$, the recirculation zones on the sides stand out from the recirculation zone downstream of the cube. However, when α increases, both begin interacting, which gives the wake observable in figure 13. Our results illustrate that the impact of the incidence angle on the wake has a certain turbulence rate independence.

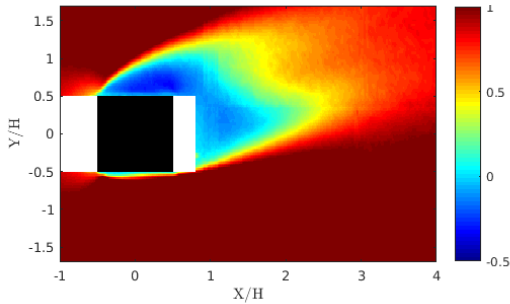


Fig. 13: U_{mean} , ($TI = 15\%$), horizontal field

Using similar considerations plus a 15° projection on the axis of the flow, the calculations give $x_{ds}/H^* = 1.4$. H^* is the projected area of the cube: $H^* = H\sqrt{2} \cdot \cos(45 - \alpha^\circ)$. However, since the wake no longer is drop shape, it would be more interesting to look at the width w_{ds} rather than the length of the recirculation area downstream of the cube. In this paper, w_{ds} is calculated for $z/H = 0.7$ and is defined as the area where $U_{mean} < 0$. For case 1a, $w_{ds}/H = 1.1$ at $x/H = 1$ (where the wake is the widest). For case 2, we find $w_{ds}/H^* = 1.2$. w_{ds} is calculated at a distance H from the centre of the projected impact surface of the cube. The wake is then slightly wider for the degraded flow.

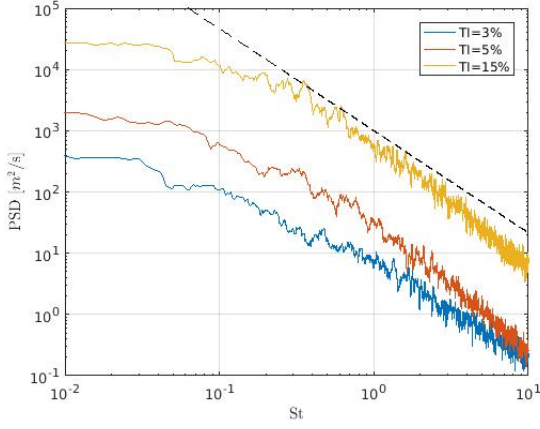
At $x/H = 3$ and $y/H = 0$, in figure 13, we find $U_{mean} \sim U_\infty/2$. But, for case 1a, in figure 7(a), $U_{mean} < U_\infty/2$. Hence, in case 2 the flow reforms faster than in case 1a, the wake behind the cube is then

shorter. It is mostly caused by the incidence since similar results can be found in [23] where, for similar incoming conditions, the recirculation zone weakens when α increases. This could also be explained by the fact that, in a highly turbulent flow, the wake dissipates faster.

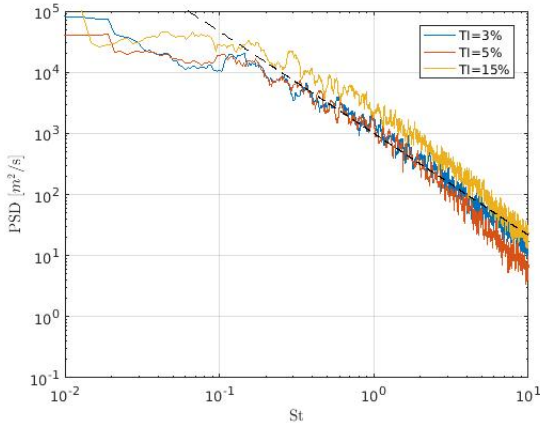
B. Time series analysis

In this section, the LDV measurements are used. Indeed, LDV acquisitions are made for long acquisition time worth high acquisition frequencies up to $100 Hz$, whereas PIV measurements are at fixed acquisition frequency of $15 Hz$. The PSD plotted against the Strouhal number ($S_t = \frac{fH}{U_\infty}$) are presented in figure 14(a) upstream of the cube ($x/H = -2$) and in figure 14(b) downstream of the cube ($x/H = 2$) both at $y/H = 0$ and $z/H = 0.75$. These curves are compared with the $-5/3$ decreasing slope of the Kolmogorov theory describing the conservation of energy between the production and dissipation scales. The PSD spectra of each case obey the $-5/3$ law for different frequency ranges: $[S_t = 1.5; S_t = 10]$ for case 1a, $[S_t = 0.4; S_t = 3]$ for case 1b and $[S_t = 0.3; S_t = 2]$ for case 2. It appears that the frequency range of energy conservation described by Kolmogorov decreases for increasing turbulence intensity. Another interesting aspect is the clear difference of the PSD spectra upstream and downstream of the cube. Upstream, the amplitude is proportional to the turbulence intensity, the incoming flow governs the global behaviour. Downstream, all PSD spectra overlap. The amplitude increase is caused by the turbulence intensity increase: in the wake of the cube, the agitation is such that fluctuating velocities are higher. The overlapping of all three spectra indicates that the flow is governed by the wake of the cube. This is a clear illustration of the impact of a wall-mounted cube in a turbulent flow.

The PSD spectra for the spanwise fluctuating velocity v' is shown in figure 15 upstream ($x/H = 2$) and downstream ($x/H = -2$, $y/H = 0$ and $z/H = 0.75$). Looking at the spanwise velocity rather than the streamwise velocities better reveals the vortices passing and allows to bring out a peak at $S_t = 0.09$. This is a common value in the literature ([24], [25], [16] and [14]) which usually indicates the shedding of vortices in the flow (see fig. 5(a) and table III). On the whole domain, it is clearly marked for case 1a, less for case 1b and can no longer be seen for case 2 (using the Fast Fourier Transform and with the measurement planes available here). Increasing the turbulence causes dissipation through particular agitation that hides the vortex shedding phenomenon. Furthermore, the observation of the vortex shedding frequency can be a way of estimating the area of influence of the cube. Maps of dominating S_t against y or z are produced and a new evaluation of the zone of influence of the cube is made. We find that for both cases 1a and 1b: $y_{i,2}/H = 2$ and $z_{i,2}/H = 1.5$. These results are higher than the one obtained with the considerations on U_{mean} .



(a) PSD of u' upstream of the cube ($x/H = -2$, $y/H = 0$ and $z/H = 0.75$)



(b) PSD of u' downstream of the cube ($x/H = 2$, $y/H = 0$ and $z/H = 0.75$)

Fig. 14: Influence of the cube on the PSD of u' at different TI . Dotted line is a $-5/3$ slope.

In section III, experiments on a wall-mounted cube were performed at $Re = 2.5 \cdot 10^5$ and $Fr = 0.23$. The results, for all three types of incoming flows were consistent with the results found in the literature. The cube is a good introduction to the turbulence characterization project since it helps defining the incoming conditions in the tank and developing analysis tools. The conclusions on the impact of turbulence on the wake of the cube will be used for conclusions in the future experiments. However, no structure were persistent enough to go up the water column and to create a perturbation on the free surface in the tank. Other experiments on sequences of obstacles can be found in the literature. For example, [26] studied complete canopies. However, the Reynolds number was lower, no turbulent structure going high enough was detected. Neither the wall-mounted cube alone nor sequences of cubes allow to characterize the turbulence in the Raz Blanchard; a new type of experiment needs to be achieved.

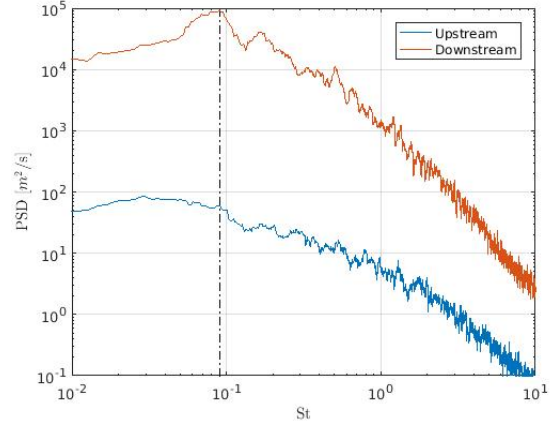


Fig. 15: Observation of the shedding frequency on the power spectrum density of v' , upstream ($x/H = -2$) and downstream ($x/H = 2$) of the cube. Dots indicate $St = 0.09$.

IV. NEW EXPERIMENTAL SET UP

A. Description of the phenomenon

As explained in the introduction part, some particular turbulent structures can create boils at the sea surface, these structures are called Kolk vortices. It is likely that such phenomena occur in the Raz-Blanchard and their existence could give information about the topology of the flow *in-situ*. In [10], it is explained that Kolk vortices are caused by the flow separation occurring at the upstream edge of the first dune. They originate at the reattachment line on the crest of the following dune (see figure 16). Due to the turbulent aspect of the incoming flow, the intermittency of the reattachment point causes the development of a 3D structure: a horseshoe vortex that is highly energetic and rises up to the free surface.

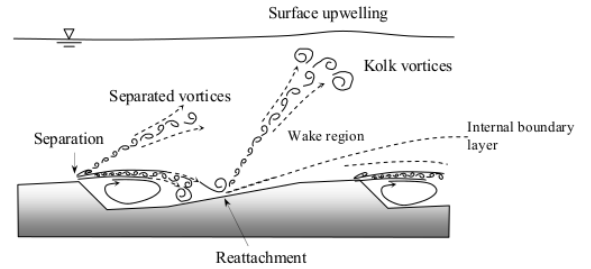


Fig. 16: Apparition of Kolk Vortices and boils from [10]

Based on the bibliographic work, the rise of the Kolk vortex seems to be caused by the existence of a reattachment line behind obstacles with high aspect ratio ($A_R = \frac{\text{width}}{\text{height}}$) like dunes and the fact that the flow reattaches on a inclined surface (from 2° to 5°). Unlike the wall-mounted cube, on structure with higher A_R , the side vortices have less influence on the recirculating region. In [17], it was found that for $A_R > 6$, a 2D region exists downstream of the obstacle and the reattachment becomes a line.

B. Slope impact behind low A_R obstacles

When studying the example of Kolk vortices, two phenomena are identified in the production of persistent vortices: the presence of an inclined surface downstream of the obstacle and the high A_R of the dune shaped obstacle. It might be possible that the simple existence of an inclined floor downstream of any obstacle could impulse coherent turbulent structures to the free-surface.

Experimental tests are carried out with the same wall-mounted cube and experimental conditions ($U_\infty = 1\text{ m/s}$ and $TI = 3\%$). A 1.2 m wide 6.5° inclined floor is installed downstream of the cube (see fig. 17). The 6 PIV measurement planes have a spatial discretization of 0.26 mm in both directions. The camera acquires 2250 double images separated by $800\ \mu\text{m}$ at $f_e = 15\text{ Hz}$. The previous configuration (cube alone) is referred to as case 1a and the present one (cube with a 6.5° inclined floor) as case $1a_{slope}$.

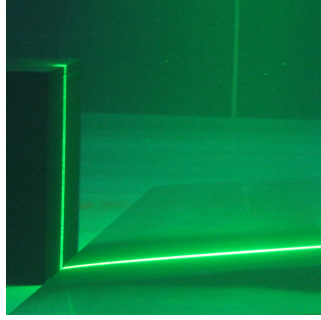


Fig. 17: Representation of the cube and the 6.5° inclined floor in the tank

Figure 18 illustrates that the inclined floor has a strong impact on the form of the recirculation region (compared to the case 1a in figure 5(a)). It gives an impulsion to the flow that causes the appearance of a region where $W_{mean} > 0$ at the bottom of the recirculation zone ($x/H = 1.7$ and $z/H \in [0.2; 0.7]$) and a stagnation point appears at $x/H = 1.7$, $z/H = 0.7$. As a preliminary analysis, the product of the instantaneous fluctuating velocity components $u'w'$ is plotted in figure 19 at four different points³: A $_{(1.4)}^{(2.3)}$ B $_{(1.4)}^{(3)}$ C $_{(1.8)}^{(2.3)}$ D $_{(1.8)}^{(3)}$ (see fig. 18). Figure 19 shows that the fluctuations are higher for case $1a_{slope}$: $|u'w'|_{max} = 4 \cdot 10^{-2}\text{ m}^2/\text{s}^2$ in case $1a_{slope}$ and $|u'w'|_{max} = 2.5 \cdot 10^{-2}\text{ m}^2/\text{s}^2$ in case 1a. In case 1a, only points A&B see the highly turbulent wake of the obstacle, the signals for points C&D show undisturbed flow ($|u'w'|_{C\&D} < 1 \cdot 10^{-3}\text{ m}^2/\text{s}^2$). However, in case $1a_{slope}$, C&D see higher velocities fluctuations: $|u'w'|_{C\&D} > 1 \cdot 10^{-2}\text{ m}^2/\text{s}^2$. It illustrates how the turbulent structures created by the cube presence are impulsed higher into the water column by the inclined floor.

In figure 20, the most significant ejection type event ($u' < 0$ and $w' > 0$) was selected. For both cases, w' is plotted for an observation window represented in figure 18. It is observed that each $w' > 0$ event (red) is preceded by a $w' < 0$ event (blue). It is in agreement with the results in

³In $(\frac{x}{H}, \frac{z}{H})$ coordinates

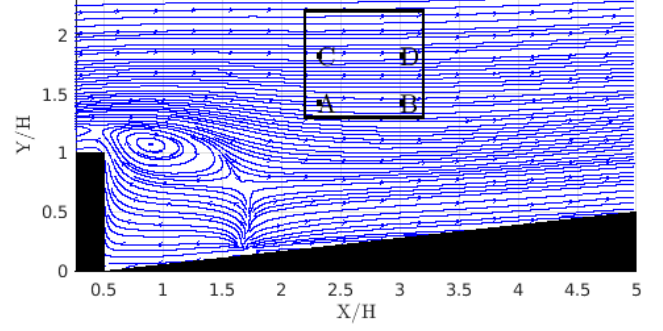


Fig. 18: Streamlines for case $1a_{slope}$. Rectangle represents the observation window for fig. 20 and points A B C D for fig. 19

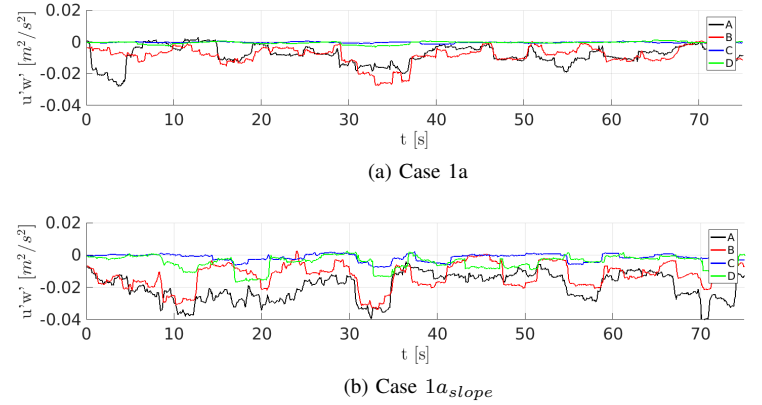


Fig. 19: Signals of $u'w'$ (PIV measurements) for $t \in [0; 75]\text{ s}$

[6]: "as low-momentum fluid is ejected away from the bed, fluid from higher in the flow is induced to move towards the bed in order to satisfy continuity.". Figure 20 illustrates once more that the ejection is stronger ($w'_{1a_{slope}} > w'_{1a}$) at its maximal value when impulsed by an inclined floor. The turbulent structures reach higher altitudes when impulsed. A 13% increase is measured for in case $1a_{slope}$ ($z_i/H = 1.7$) compared to the case 1a ($z_i/H = 1.5$).

Hence, the existence of an 6.5° inclined floor behind the cube has a major impact on the wake of the cube. It changes the form of the recirculation area, the flow is redirected towards the free surface rather than the bottom and it causes the apparition of a stagnation point at $z/H = 0.7$. It also impacts the propagation of coherent turbulent structures that reach higher location in the water column (up to 13% higher). It is shown that the inclined floor is partly responsible for the rise of vortices. However, in this set of experiments, no boils are observed at the free surface.

C. Slope impact behind high A_R obstacles

Kolk vortices have been exclusively observed behind obstacles with high A_R such as dunes. The slope effect of the

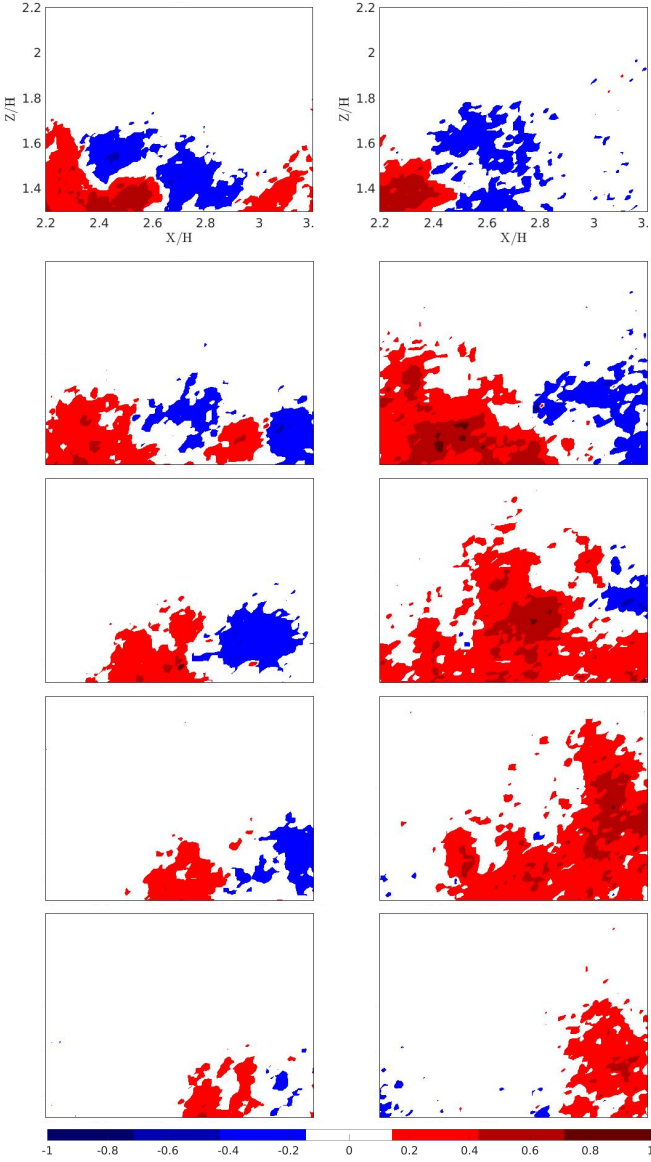


Fig. 20: Maps of consecutive instantaneous w' during $8s$, $x/H \in [2.2, 3.2]$, $z/H \in [1.3, 2.2]$. Case 1a (left) and case $1a_{slope}$ (right)

dune on the creation of Kolk vortices is investigated with the use of a numerical model developed on TELEMAC 3D [20]. A simple case on dunes is computed for $U_\infty = 0.57 \text{ m/s}$ and $TI = 15\%$. The ratio $\frac{\text{Dune height}}{\text{Depth}} = \frac{1}{4}$ is consistent with the literature on Kolk vortices. The spanwise vorticity field is presented in figure 21. It shows vortices that go up to twice the dune height behind the dune. The first simulations on simple dune cases give some very persistent structures that rise up to the free surface. These are encouraging results and the model will continue to be developed to extend the results presented here to real-life cases. In parallel, we shall develop an experimental set up to re-create these structures behind high A_R obstacles with an inclined floor downstream. The

experimental work carried out in the tank should be then considered as a database for validation of the numerical model.

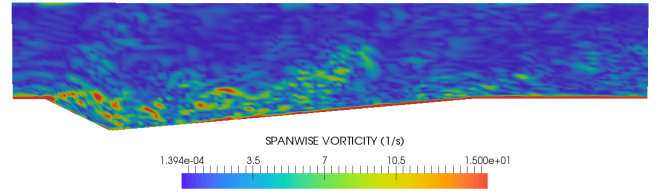


Fig. 21: Simulation on dunes with a 5° slope, $Re = 3.3 \times 10^5$ and $Fr = 0.23$. Isosurfaces of the spanwise vorticity field. [20]

So far, thanks to experimental results, simple observations on the average velocity and the vorticity fields were made. More evolved techniques for the observation of the free surface (techniques developed in [10]) can be used. Also, a more extensive frequency analysis should be done since it was proven that the frequency of Kolk vortices is lower than the vortex shedding frequency ([9]). These techniques will support the identification of roughness-free-surface interactions.

V. CONCLUSION

In order to understand the turbulence phenomena existing in the Raz-Blanchard, elements of the real bathymetry were experimented. First, the case of a wall-mounted cube, representing the mean bathymetric variation encountered in this area, has been investigated. The experiments have been carried out at $Re = 2.5 \times 10^5$ and $Fr = 0.23$ and for various turbulence level. Results show that, for low turbulence levels ($TI = 3\%$ and $TI = 5\%$), the flow around the obstacle has similar behaviour: the cube has an influence of $1.5H$ on the external flow and the downstream reattachment point is located at $x/H = 1.9$ in both cases. Experimental results were similar to the literature. These results and those found in the literature have then been compared to a degraded case with an incoming $TI = 15\%$ and a 15° incidence angle. Finally, a time series on lower TI analysis revealed the vortex shedding frequency at $S_t = 0.09$ which is a typical value extensively present in the literature.

In-situ, large boils can be observed at the sea surface. Such boils could be caused by large-scale turbulent events that originate at the sea bottom. One of the possible explanation found in the literature are Kolk vortices created by large-scale dunes at the sea bottom. The problem is separated into two parts: the inclined floor downstream of the obstacle and the large aspect ratio of the dunes. In order to recreate more realistic structures, a way of impulsing the turbulent structures higher into the water column was proposed. A 6.5° inclined floor has been installed downstream of the cube for the same upstream conditions. It was found that a stagnation point appears in the wake of the cube, on the limit of the recirculation region. It causes ejection events to be observed 13% higher in the water column than those observed without

the inclined floor. The case of dune was then investigated numerically and give qualitatively similar behaviour of very persistent turbulent structures in the wake of the obstacle. An obstacle with high aspect ratio will be tested in the tank and the influence of the slope of the inclined floor and the incoming turbulence intensity will be investigated.

ACKNOWLEDGEMENT

The authors acknowledge the financial support of IFREMER and the Hauts de France Regional Council for this PhD study. We are most grateful to Thomas Bacchetti and Jean-Valery Faq for their assistance and precious advices. The authors are also grateful to Adrien Bourgoïn who provided the numerical results presented in this paper.

REFERENCES

- [1] A. Day, A. Babarit, A. Fontaine, Y.-P. He, M. Kraskowski, M. Murai, I. Penesis, F. Salvatore, and H.-K. Shin, "Hydrodynamic modelling of marine renewable energy devices: A state of the art review," *Ocean Engineering*, vol. 108, pp. 46–69, 2015.
- [2] H. Boyé, E. Caquot, P. Clment, L. De La Cochetière, J.-M. Nataf, and P. Sergent, "Rapport de la missions d'étude sur les énergies marines renouvelables," 2013.
- [3] SHOM, "MNT bathymétrie de façade atlantique (projet homonim)," 2015.
- [4] P. Mycek, B. Gaurier, G. Germain, G. Pinon, and E. Rivolaen, "Experimental study of the turbulence intensity effects on marine current turbines behaviour. part I: One single turbine," *Renewable Energy*, vol. 66, pp. 729–746, 2014.
- [5] R. Kostaschuk and M. Church, "Macroturbulence generated by dunes: Fraser river, canada," *Sedimentary Geology*, vol. 85, pp. 25–37, 1993.
- [6] J. Best, "Kinematics, topology and significance of dune-related macroturbulence: some observations from the laboratory and field," *Spec. Publs int. Ass. Sediment*, vol. 35, pp. 41–60, 2005.
- [7] J. Best, "The fluid dynamics of river dunes: A review and some future research directions," *J. Geophys. Res.*, vol. 110, 2005.
- [8] G. Matthes, "Macroturbulence in naturel stream flow," *Transactions, American Geophysical Union*, vol. 28, pp. 255–265, 1947.
- [9] A. Kadota and I. Nezu, "Three-dimensional structure of space-time correlation on coherent vortices generated behind dune crest," *J. Hydraul. Eng.*, vol. 37, pp. 59–80, 1999.
- [10] C. Polatel, "Large-scale roughness effect on free-surface and bulk flow characteristics in open-channel flows," Ph.D. dissertation, The University of Iowa, 2006.
- [11] H. Ha and S. Chough, "Intermittent turbulent events over sandy current ripples: a motion-picture analysis of flume experiments," *Sedimentary Geology*, vol. 161, pp. 295–308, 2003.
- [12] T. Stoesser, C. Braun, M. García-Villalba, and W. Rodi, "Turbulence structures in flow over two-dimensional dunes," *J. Hydraul. Eng.*, vol. 134, pp. 42–55, 2008.
- [13] D. Grigoriadis, E. Balaras, and A. Dimas, "Large-eddy simulations of unidirectional water flow over dunes," *J. Geophys. Res.*, vol. 114, 2009.
- [14] R. J. Hearst and B. Gomit, G.and Ganapathisubramani, "Effect of turbulence on the wake of a wall-mounted cube," *J. Fluid Mech.*, vol. 804, pp. 513–530, 2016.
- [15] I. Castro and A. Robins, "The flow around a surface-mounted cube in uniform and turbulent streams," *J. Fluid Mech.*, vol. 79, pp. 307–335, 1977.
- [16] H. Hussein and R. Martinuzzi, "Energy balance for turbulent flow around a surface mounted cube placed in a channel," *Phys. Fluids*, vol. 8, pp. 764–780, 1996.
- [17] R. Martinuzzi and C. Tropea, "The flow around surface-mounted, prismatic obstacles placed in a fully developed channel flow, (*Data Bank Contribution*)," *J. Fluid Eng.*, vol. 115, pp. 85–92, 1993.
- [18] B. Van Oudheusden, F. Scarano, N. Van Hinsberg, and D. Watt, "Phase-resolved characterization of vortex shedding in the near wake of a square-section cylinder at incidence," *Experiments in Fluids*, vol. 39, pp. 86–98, 2005.
- [19] M. Grondeau, P. Mercier, S. Guillou, Y. Méar, J. Poirier, and E. Poizot, "Lattice boltzmann method turbulence modeling for tidal power environment simulation," *Journées de l'Hydrodynamique*, 2016.
- [20] A. Bourgoïn, S. Guillou, J. Thiébot, R. Ata, and S. Benhamadouche, "Development of a large-scale eddy simulation approach for tidal currents modelling," *EWTEC*, 2017.
- [21] O. Duràn Medina, F. Schmitt, R. Calif, G. Germain, and B. Gaurier, "Correlation between synchronised power and flow measurements, a way to characterize turbulent effects on a marine current turbine," *EWTEC*, 2015.
- [22] J. Wood, S. De Nayer, G.and Schmidt, and M. Breuer, "Experimental investigation and large-eddy simulation of the turbulent flow past a smooth and rigid hemisphere," *Flow Turbulence Combust*, vol. 1, pp. 79–119, 2016.
- [23] N. Saïd, H. Mhiri, P. Caminat, G. Le Palec, and P. Bournot, "Wind tunnel investigation and numerical simulation of the near wake dynamics for rectangular obstacles," *Env. Eng. Science*, vol. 25, pp. 1037–1060, 2007.
- [24] P. Sattari, J. Bourgeois, and R. Martinuzzi, "On the vortex dynamics in the wake of a finite surface-mounted square cylinder," *Exp Fluids*, vol. 52, pp. 1149–1167, 2012.
- [25] H. Wang and Y. Zhou, "The finite-length cylinder near wake," *J. Fluid Mech.*, vol. 638, pp. 453–490, 2009.
- [26] E. Florens, O. Eiff, and F. Moulin, "Defining the roughness sublayer and its turbulent statistics," *Experiments in Fluids*, vol. 54, pp. 1–15, 2013.